PAPER • OPEN ACCESS

Design and construction of the ATEFA facility for experimental investigations of AMTEC test modules

Design and construction of the ATEFA facility for experimental investigations of AMTEC test modules

N Diez de los Rios Ramos[1,4], W Hering[1], A Weisenburger[2], M Stüber[3], A Onea[1], M Lux[1], S Ulrich[3] and R Stieglitz[1]

[1]Institute for Neutron Physics and Reactor Technology (INR), Karlsruhe Institute of Technology (KIT), Hermann-von-Helmholtz-Platz 1, 76344 Eggenstein-Leopoldshafen, Germany
[2]Institute for Pulsed Power and Microwave Technology (IHM), Karlsruhe Institute of Technology (KIT),
[3]Institute for Applied Materials – Applied Materials Physics (IAM-AWP), Karlsruhe Institute of Technology (KIT)
[4]nerea.diez@kit.edu

Abstract. The Alkali Metal Thermal-to-Electric Converter (AMTEC) is an electrochemical cell that requires a high temperature heat source to generate electricity. At KIT the AMTEC technology is being investigated focusing on the use of concentrating solar energy as heat source. First a review on AMTEC technology is given. Further, the design and realization phases of the AMTEC Test Facility (ATEFA) and AMTEC test cell are presented, including the data acquisition and control system and two key technology developments: a ceramic to metal joint for high temperatures (800 – 1000 °C) and the magnetron sputtering of cathode layers on the ceramic electrolyte. The sheet resistance of several electrode samples has been analyzed using the 4-point probe technique and the microstructure of the cathode layer has been examined using the scanning electron microscopy (SEM).

1. Introduction

Liquid metals are possible candidates for expanding the temperature application range in concentrating solar power (CSP) plants and thus leading to an increased efficiency of central tower solar systems. The same objective can be supported by the Alkali Metal Thermal-to-Electric Converter (AMTEC), which operates with sodium in two main modes: liquid- or vapor-anode modes depending on the applied temperature range (up to 800 – 1000 °C).

At Karlsruhe Institute of Technology (KIT) the AMTEC technology is being investigated focusing on the use of concentrating solar energy as heat source of the electrochemical converter. The concept proposed by Hering et al. [1] uses liquid metals such as sodium for a hybrid CSP plant combined with the AMTEC technology. The system should increase the overall efficiency of the power plant compared to conventional CSP systems. As first step towards the present concept, several liquid sodium facilities have been designed and constructed at the Institute for Neutron Physics and Reactor Technology (INR) – KIT [2]; in particular the AMTEC Test Facility (ATEFA) serves for research on single AMTEC test cell characteristics and performance evaluation, as well as process optimization in short term tests. A SOLTEC (SOdium Loop to TEst materials and Corrosion) facility has also been designed at INR-KIT for long term tests on power degradation issues [3].

Taking into consideration the main developments reported in the literature on AMTEC cells and the still existing challenges, a basic single cell design was proposed based on the work of Heinzel et al. [4]. The aim of the present work was to develop the layout and engineering solutions to construct the AMTEC Test Facility (ATEFA) and AMTEC test cell using new available technologies within the Helmholtz AMTEC Center (HAC).

2. Alkali Metal Thermal to Electric Converter (AMTEC)
AMTEC, originally called Sodium-Heat-Engine, arose in the sixties at the Ford Motor Company as a spinoff of the sodium-sulfur-battery and was further investigated at the Jet Propulsion Laboratory (JPL) [5] focusing on electrical power generation mainly for spacecraft operations. Already in the '90s AMTEC was a promising power conversion device for space missions thanks to its fast development.

In Germany, the group of Heinzel at the Forschungszentrum Karlsruhe (presently KIT) worked in cooperation with the Asea Brown Boveri (ABB) in several AMTEC experimental studies for terrestrial applications, especially for CSP applications. Elaborated tests were made from 1991 until 1993 to analyze different electrodes, current collectors and current leads [6].

Several authors observed that the conductivity of the electrolyte decreased over time, influencing significantly the power output. Lodhi et al. [7] found that during the first 7000 h of operation almost the entire power loss was attributable to the ionic resistance of the ceramic electrolyte. After that, other components like electrodes began to be relevant in the power degradation mechanisms too. At the end of 12000 h, the ionic resistance of the electrolyte represented 58 % of the total cell resistance.

Contrary to the disclosed results, Hunt and Rasmussen [8] reported in 2006 the long term constant performance of a small, multi-tube AMTEC over 5 years of continuous operation. This result shows the first AMTEC cell operated over several years without power degradation. Although no explanation is given by the authors to these positive results, one possible reason is the operation at relative low temperature and very low current density of < 1.4 A/cm^2.

2.1. Operating principle
AMTEC is a concentration cell that uses an alkali metal such as sodium and a high temperature heat source to generate DC electricity. The key component is the ß''-alumina solid electrolyte (BASE) that is able to conduct sodium ions while acting as a barrier for electrons. The high temperatures (600 – 1000 °C) in the cell are needed for an improved ion transport in the ceramic electrolyte. The BASE separates the cell into the anode side, where sodium is heated up and pressurized to $0.1 - 0.2$ MPa, and the cathode side that contains sodium vapor at much lower pressure ($\sim$ 100 Pa) and temperature ($<$ 400 °C).

The pressure difference applied across the electrolyte generates an electrochemical disequilibrium. As a result the system tends to balance it by reducing sodium atoms at the anode surface and further diffusion of sodium ions through the electrolyte to the cathode surface. When connecting electrically both sides of the cell, electrons set free in the sodium reduction travel through an external load from the anode to the cathode generating thereby electricity. After reaching the cathode surface, electrons recombine with sodium ions to give sodium vapor. The redox equation for AMTEC cells is based on the sodium ionization:

$$Na \leftrightarrow Na^+ + e^- \tag{1}$$

Since the oxidation and reduction products in AMTEC are the same, AMTEC cells can be considered a "zero" net fuel consumption technology if the obtained sodium at the cathode is condensed and directed back to the anode for instance by means of an electromagnetic pump or a wick that uses capillary forces.

If no electrical charge exchange between electrodes is allowed, an open circuit voltage (OCV) arises in the system at electrochemical equilibrium. The theoretical OCV for an AMTEC cell is represented by the Nernst equation (2) in terms of the sodium vapor pressure at the anode and cathode, p_a^{oc}, p_c^{oc}.

$$V^{oc} = \frac{RT_B}{F} \ln\left[p_a^{oc}/p_c^{oc}\right] \qquad (2)$$

where T_B represents the temperature of the BASE, R the gas constant and F the Faraday constant. The values obtained with the Nernst equation are considered to be the maximum for the ideal case. Typical measured values are $V^{oc} = 0.6 - 1.2$ V.

The two main issues related to AMTEC devices that require further investigations are the lower real efficiency (~ 20 % at > 800 °C) [9] compared to the theoretical value (~ 45 % at > 800 °C) [6] and power degradation occurring in long time operation due to changes in BASE and electrodes.

2.2. Polarization and cell losses
The isothermal cycle of AMTEC approximates the Carnot cycle and therefore the theoretical efficiency of AMTEC can reach high values of about ~ 45 %. This also means that the temperature difference between BASE and condenser and therefore the heat losses play an important role in a coaxial configuration of the cell (see Figure 5). Heat radiation losses can be reduced for instance by adding radiation shields or by using the condensed molten sodium film on the condenser surface as radiation shield.

Figure 1 shows typical characteristic curve of a coaxial AMTEC cell from an electrochemical point of view and reflects the impact of ohmic cell losses and polarization losses in the electrodes. Polarization losses in the anode are negligible thanks to the good wetting at high temperatures and the good electrical conductivity of liquid sodium. The curve has a rapid initial fall; the main source of voltage drop in this region is the activation polarization losses that appear due to the slow reaction kinetics on the surface of the electrodes. After the activation polarization region, the voltage continues decreasing with a linear slope, characteristic of the region where the increase of ohmic losses predominates. At high current densities the voltage drop increases due to the concentration polarization losses; in this region the diffusion rate of sodium vapor is considerably lower than the reaction kinetics, which leads to an increase of the sodium concentration at the surface of the cathode. Most of the reported AMTEC cells in the literature do not exhibit the concentration polarization region owing to a relative good sodium vapor transport; the linear voltage-drop region prevails even at current densities as high as 2 A/cm² and voltages of ~0.2 V.
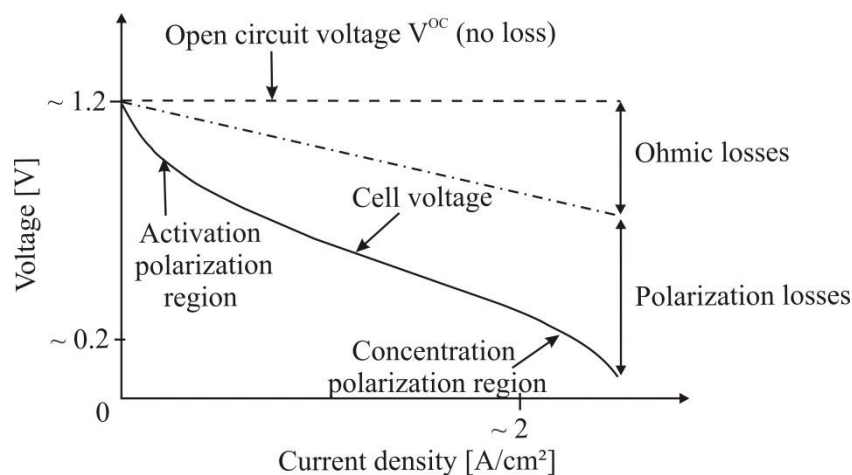
Figure 1. Representation of a typical AMTEC characteristic curve (solid line) and the electrochemical loses for a coaxial configuration of the cell.

The internal resistance of the cell is composed by the ionic resistance of the BASE (B), the electrical resistance of the electrode (e), the current collector (ic), the current leads (l) and the contact resistance (con):

$$R_{cell} = R_B + R_e + R_{ic} + R_l + R_{con} \tag{3}$$

Taking all these losses into consideration, the effective electromotive force of the cell V^{cc} can be calculated as the open-circuit voltage V^{oc} minus the voltage loss originated at anode ξ_a and cathode ξ_c and the ohmic losses ξ_r generated by the internal resistance of the cell:

$$V^{cc} = V^{oc} - \left(\xi_a - \xi_c \right) - \xi_r \tag{4}$$

Liquid-anode AMTEC cells have negligible polarization losses in the anode $\xi_a \sim 0$ thanks to the good wetting of liquid sodium at high temperatures. After an elaborated derivation of the Butler-Volmer equation and assuming that interfacial and bulk sodium and sodium-ion concentrations are equal, and that the electrochemical transfer coefficient is ½, the current density at the cathode interface J can be calculated as follows [10]:

$$J = J_0^{ex} \frac{p_B \, e^{-0.5 \, V^{cc} \, f} - p_c^{oc} \, e^{0.5 \, V^{cc} \, f}}{p_B + K_f \, J_0^{ex} \, e^{0.5 \, V^{cc} \, f}} \tag{5}$$

where $f = F / RT_B$, J_0^{ex} is the exchange current density of the cell at an equilibrium potential obtained with saturated sodium vapor in contact with the electrode, p_B, p_c^{oc} represent respectively the saturated vapor pressure of sodium at T_B and the pressure of sodium vapor at the cathode open circuit conditions, and K_f is the factor of linear pressure increment in the cathode. Clearing the cell potential V^{cc} from equation (5) and combining it with equation (4), the cell potential can be written as [10]:

$$V^{cc} = \frac{2}{f} \ln \left\{ \frac{p_B}{2 \left(J \, K_f + p_c^{oc} \right)} \left[\frac{-J}{J_0^{ex}} + \left(\left(\frac{J}{J_0^{ex}} \right)^2 + \frac{4 \left(J \, K_f + p_c^{oc} \right)}{p_B} \right)^{1/2} \right] \right\} - J \, R_{cell} \tag{6}$$

which reduces to the Nernst equation for $J = 0$. The right part of the equation (6) corresponds to the ohmic losses ξ_r and the left part of the equation (6) is the expression of the rest of the terms from equation (4): $V^{oc} - \left(\xi_a - \xi_c \right)$.

2.3. Technical implementation

AMTEC devices have five main components that are relevant for the performance of the cell: BASE electrolyte, electrodes, current collector, the working fluid and the configuration of the cell. The latter will not be addressed in this work, however it should be considered from a thermodynamic point of view for optimized AMTEC cells.

2.3.1. ß''-alumina solid electrolyte (BASE).

The BASE electrolyte emerged in the field of sodium batteries and has a complex crystal structure (see figure 2). It consist of spinel-like blocks of Al^{3+} and O^{2-} ions, built with octahedral and tetrahedral prisms, and connected to each other through Al-O-Al bonds. The large oxygen ions create "open" planes between spinel blocks, known as conduction planes, through which the conduction takes place by migration of small sodium cations vacancies. The conductivity is limited to these planes only, since the movement along the perpendicular direction is notably difficult.

There are two main BASE polycrystalline structures that have been used in AMTEC cells: ß- and ß''-alumina. They have a different stacking arrangement of the spinel blocks and conduction planes: ß-alumina has two conduction planes that act simultaneously as mirror planes and ß"-alumina has three conduction planes however these are not mirror planes. The stacking arrangement of the ß''-structure is repeated every three spinel-type blocks, while ß-alumina has a two block structure. This arrangement is responsible for the higher ion conductivity of ß''-alumina. This is the reason why materials with the ß''-structure have been widely used in AMTEC cells rather than ß-structure. Polycrystalline ß''-alumina is a non-stoichiometric ceramic and contains an excess of Na^+ ions. The

ß''-structure is stable only in the presence of ions like Li^+ and Mg^{2+}. The substitution of Al^{3+} with these stabilizers (mono- or divalent ions) balances the excessive positive charges of Na^+ and increases the conductivity of the ceramic. Single crystal structures have also been proposed in the literature, due to their higher ion conductivity compared to polycrystalline structures; however the high costs connected with synthesizing single phases make them not competitive against polycrystalline ceramics.
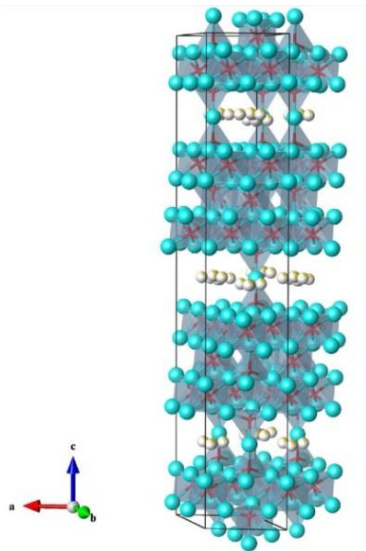
Figure 2. Crystal structure of Na-ß''-alumina. Spinel-like blocks of Al-O are separated by conduction planes, where the Na^+ and O^{2-} ions are located [11].

2.3.2. Electrode. To ensure a high current density and high efficiency, the cathode must satisfy the following properties: i) high electrical conductivity, ii) good adhesion to BASE's surface, iii) similar coefficient of thermal expansion to that of BASE, iv) high corrosion resistance to sodium vapor, v) large triple phase boundary (TPB), vi) low resistance to transport of sodium vapor, and vii) stability at high temperatures (slow grain growth and material migration). Refractory and ceramic electrode materials have been commonly used in AMTEC devices due to their suitable properties [12]; nevertheless their long-term stability at high temperatures needs to be further investigated. Table 1 classifies some of the most relevant literature results on AMTEC cells attending to electrode materials. T_{Na} represents the temperature of sodium in the anode, P_e is the power output of the cell, t_e is the thickness of the electrode and A_e the electrode area. According to the present table, materials with the highest power output seem to be Pt/W, Rh/W and TiC. However an accurate comparison requires considering identical conditions of temperature, electrode surface, current collector structure, operating time, vapor pressure, etc. Therefore further experimental tests should be performed in this field to confirm this statement. In this work TiN and TiC electrodes have been selected for coating development. Despite the lower power density of TiN compared to TiC, it is one of the electrode materials with largest documentation reported in AMTEC literature.

The morphological aspects of the cathode are directly connected with the polarization losses in AMTEC. Table 2 shows the favored grain size, porosity and thickness tendencies to decrease polarization losses. A certain porosity is needed in the cathode for a good sodium vapor transport and thus low concentration polarization; however a too large porosity can affect negatively the activation and ohmic losses. The TPB length would decrease and simultaneously the sheet resistance of the electrode will increase. Therefore an optimum morphology needs to be obtained experimentally for different materials. Detailed experimental data analysis can be found in the literature [13].

Two main factors were identified to describe the properties of different electrodes: the temperature-independent charge-exchange coefficient B_{ex} [$AK^{1/2}/Pa\ m^2$], determined experimentally, represents the ability of the electrode to recombine sodium atoms, and the electrode pressure loss factor G [-] stands for the transport process of vapor sodium in the cathode. An ideal perfect cathode should have $B_{ex} = \infty$

and $G = 0$, meaning that the length of the TPB is infinite long and the resistance to vapor transport is negligible.

Table 1. Literature review on electrode materials in AMTEC

Electrode	T_{Na} [°C]	P_e [W/cm²]	t_e [µm]	A_e [cm²]	Operation [hours]	Vacuum [Pa]	Ref.
Mo	800	0.5	1	0.5	Few	-	14
	800	0.217	1	30	Few	-	17
	927	0.62	~ 1	5	5	-	18
		0.46	~ 1		90	-	
TiN	687	0.25	5	7	Few	7 x 10^{-4} (without Na)	16
	746	0.315	-	60	-	-	17
	750	0.075	1	30	Few	-	18
		0.16	5		Few	-	
	850	0.47	15…50	6	Few	-	19
TiN/TiO2	850	~ 0.38	15…50	6	Few	-	
TiC	800	0.11	3…5	0.5…1	-	130	13
		0.4	3…5			0.07	
		0.75	5			0.5	
TiB$_2$	800	0.24	-	30	10	-	18
W	927	0.35	50	-	-	-	20
Pt/W	827	0.25	-	5	475	1 x 10^{-5} (without Na)	21
	887	0.8	0.7…1	1…5	160	7 – 8 x 10^4	22
Rh/W	817	~ 0.53	1.2	< 10	150	-	5
		0.5	1.2		500		
	857	0.8	1.5…2.5	5	160	7 x 10^{-4} (without Na)	16
NbN	800	0.12	2…3	-	-	130	13
		0.36	6			0.5	
LaB$_6$-B	800	0.54	-	-	-	40	23

Table 2. Optimum cathode-morphology factors to reduce polarization losses. Contrary effect of parameters.

	Grain Size	Porosity	Thickness
Activation polarization	Small	Small	-
Ohmic polarization	Large	Small	Large
Diffusion polarization	-	Large	Small

Current collector. A rather small number of studies are reported on the current collector morphology in the literature. Though, it has been shown to have a great impact on the power output of the cell. Knödler et al. [15] showed experimentally that large electrodes exhibit lower power densities than smaller ones. This fact was explained by a poor contact of the current collector and a non-uniform current distribution. To reduce this effect Knödler et al. [15] tested different current collector structures and confirmed the great impact on the power density. They increased power output between 50 – 100 % by improving the current collector structure. This great increase of the power output can be explained by an improved active electrode area. A poor or no contact between current collector and electrode surface in some regions favours the deviation of the current to those other regions where the contact is good due to the lower electric resistance. Therefore the active electrode surface is reduced.

Reducing the thickness of the electrode layer would decrease the losses due to sodium vapor transport; however the sheet resistance and thus the total resistance of the cell would increase too. Therefore an ideal current collector should have an infinite number of contact points with the electrode to compensate the high electric sheet resistance of the electrode. Moreover the current collector should have gradual structure (increasing thickness of the wires and decreasing number of wires until reaching the current lead), made of a single piece in order to eliminate internal contact resistances and simultaneously to have a good porosity to allow a free transport of sodium vapor.

Due to the cylindrical geometry of the ceramic electrolyte, obtaining a good mechanical (and therefore electrical) contact to the electrode surface becomes a challenging issue. Here small tolerances in geometry and tightness between electrode and current collector influence significantly the final contact resistance, which predominates among the electric losses. An experimental study of different current collector structures was carried out, which confirmed large significance of the contact resistance in a cylindrical AMTEC cell. Tests were performed under standard ambient conditions (25 °C, 1 atm, air) and assuming a copper rod as an ideal electrode. Among the tested current collectors, the knitted mesh used to contact directly the electrode seems to be promising thanks to the malleability of the structure that is given independently of the material properties. These results need to be still validated for AMTEC conditions at high temperature and sodium vapor environment.

2.3.3. Alkali metals for AMTEC. Sodium and potassium can be considered the best candidates as working fluid in AMTEC cells due to their favorable physical properties. There is an extensive experience in AMTEC working with sodium as opposed to potassium, which has not been yet widely spread as working fluid especially ought to the difficulties in manufacturing K-BASE electrolyte with common techniques (very high vapor pressure of K_2O at very high sintering temperatures) and to the rather limited database on the use of potassium cells. Nevertheless the interest in K-AMTEC cells is growing since 2000 thanks to the vapor phase method developed by Virkar et al. [24].

The most notable advantages of sodium compared to potassium are: i) the higher surface tension in fluid state supports the capillary process (used to form a radiation shield with liquid sodium), ii) the lower molecular weight that helps also the capillary process and decreases the pressure losses on the cathode side and iii) the ionic resistivity of the BASE is about three times lower than that of the K-BASE at ~ 1100 °C. Potassium has also several advantages: i) the higher vapor pressure (120 kPa at 1050K versus 35 kPa for Na) allows a higher anode vapor-pressure and a lower hot temperature, ii) smaller latent heat of vaporization, which reduces the thermal heat input and lowers source temperature in vapor-anode cells, and iii) lower specific heat capacity of liquid potassium.
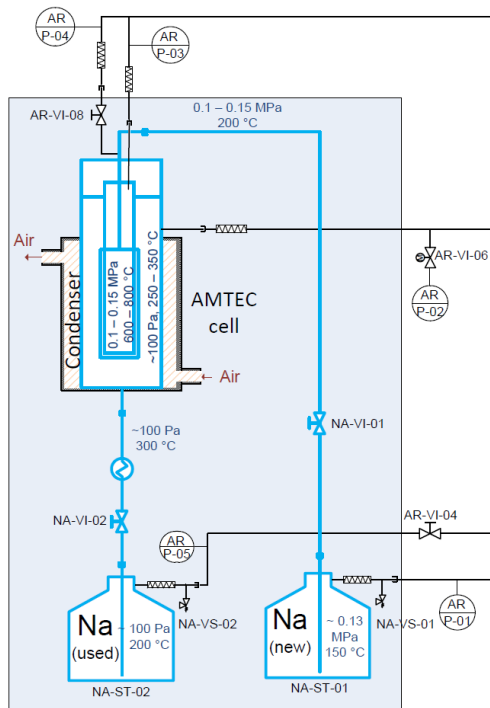
In this work sodium was selected based on the following reasons: i) the advantages of sodium properties in AMTEC mentioned above, ii) the excellent properties of sodium as heat transfer fluid for CSP, and iii) the background knowledge available in Na-AMTEC at the institute.
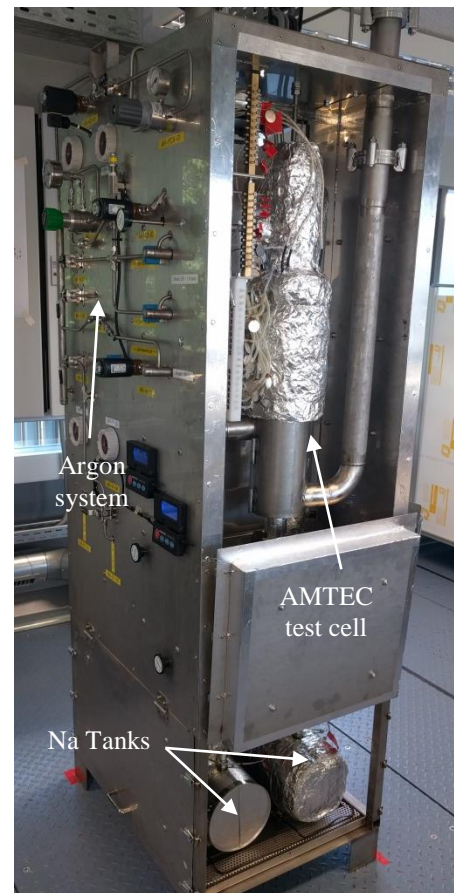
3. Experimental setup.
The main target of the work was the development and construction of the ATEFA and the AMTEC test cell [25, 26]. A detailed description of the facility and test cell is given in this chapter.

3.1. ATEFA
ATEFA is a liquid sodium facility developed for research on AMTEC technology. It was built to operate at a maximum temperature of 1000 °C and a maximum pressure of 1.7 bar during rather short term experiments, limited to a total sodium content of 3 liters. Figure 3 shows the piping and instrumentation diagram of the sodium loop in ATEFA. Sodium is driven by pressurized argon from a first tank (NA-ST-01) into the AMTEC cell; where it is heated up to 800 – 1000 °C inside the ceramic. After the diffusion through the electrolyte, sodium vapor is cooled down on the condenser surface (air cooled loop) and collected in a secondary tank (NA-ST-02). Purification of sodium takes place at the cold trap located in the KASOLA facility at INR-KIT [27].

LIMTECH

IOP Conf. Series: Materials Science and Engineering **228** (2017) 012014

IOP Publishing

doi:10.1088/1757-899X/228/1/012014

Figure 3. Piping and instrumentation diagramm of the sodium loop in ATEFA.

Figure 4. ATEFA with opened containment. Argon system is located outside the containment and sodium system inside the containment.

ATEFA is characterized by a compact construction, which is enclosed in a containment of 1.9 m height and 0.8 m width (see figure 4). The sodium system that includes the AMTEC test cell and the two sodium tanks is insulated through double metallic walls and thus physically separated from the argon system, which is located outside the containment. The argon system serves to control the mass flow rate and pressure of sodium in cell and tanks. All manual valves and displays of the sensors are located on a panel for an easy handling.

During operation, sodium is maintained molten at 150 - 200 °C in tanks and piping thanks to a heat tracing system. The highest temperature of 1000 °C is reached only inside the ceramic electrolyte and is therefore isolated from the rest of the system. Different structural materials were chosen according to the working conditions to which they will be subjected. For the low temperature region, stainless steel EN 1.4571 was selected due to its suitability in corrosive mediums. In the high temperature region of the cell, where corrosion effects are considerably more pronounced, nickel based alloys (EN 2.4663) and ceramics were considered.

Among the safety considered measures in the design and construction phases are a low sodium content of ~ 0.3 liters in the facility (without tanks), a low maximum pressure in the sodium system, the high temperature region restricted only to the ceramic electrolyte and the construction of a physical and thermal barrier between the sodium system and the operators thanks to the metallic containment (see figure 4). At any malfunction or in case of a leakage operational safety is provided through: i) a constant supervision of temperature and pressure in the system, ii) a rapid draining of sodium into the tanks (~10 seconds), iii) the possibility of floating the metallic containment with argon, iv) a

ventilation system installed in the laboratory coupled to an oxygen sensor that will activate the suction of aerosols and argon excess out of the laboratory, v) an emergency shutdown of the facility and as ultimate measure, vi) the collection of leaked sodium in a metallic sump located on the bottom of the facility containment that will provide a fast freezing.

3.2. AMTEC test cell

The structure of the cell was designed to allow a simple assembly and disassembly of all parts and defines a favorable handling of each component of the cell (see figures 5 − 7). The central part of the AMTEC test cell is the BASE, which has a tube form (D_{out} = 32 mm) and is closed at the lower end. The cell is divided by the BASE in two main regions: the inner side of the tube is filled up with liquid sodium anode and the outer surface of the tube is coated with a thin porous and electric conductive cathode.

The ceramic electrolyte is held by a niobium transition part welded to the metallic structure of the cell. The cell will be heated up through an electrical resistance. A current lead is submerged in molten sodium and collects the electrons from the anode. Three porous cathodes of ~ 45 cm² were placed on the outer surface of the BASE by reactive d.c. magnetron sputtering. The outer cell containment represents the condenser and is cooled by air.

Titanium carbide (TiC) has been selected in this work as cathode material due to the similar coefficient of thermal expansion with that of the BASE and the good results reported in the literature [8]. Current collectors were used to reduce the sheet resistance of the thin cathodes and spread the electrons homogeneously over the cathode surface. They consist of a nickel foam fastened with nickel porous sheet around the BASE tube.
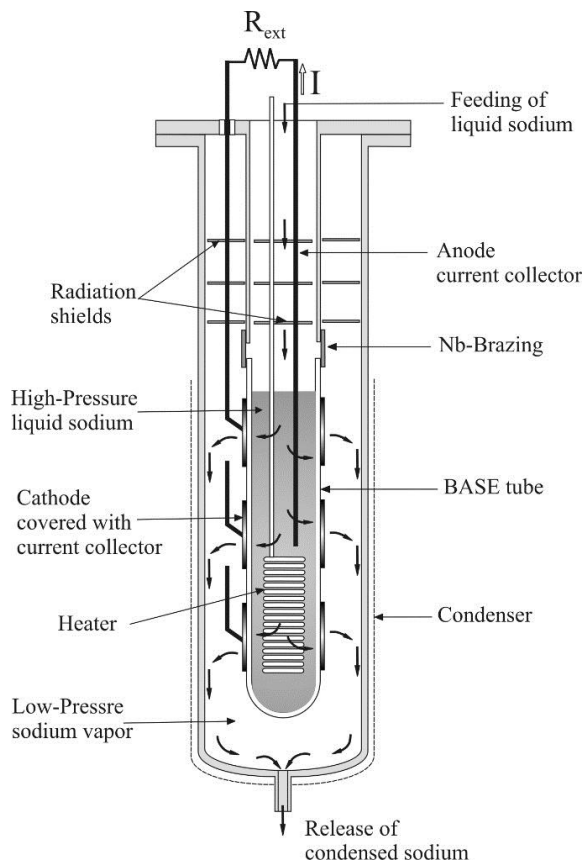
Figure 5. Schematic representation of AMTEC test cell components.

Figure 6. AMTEC test cell with integrated cooling system.
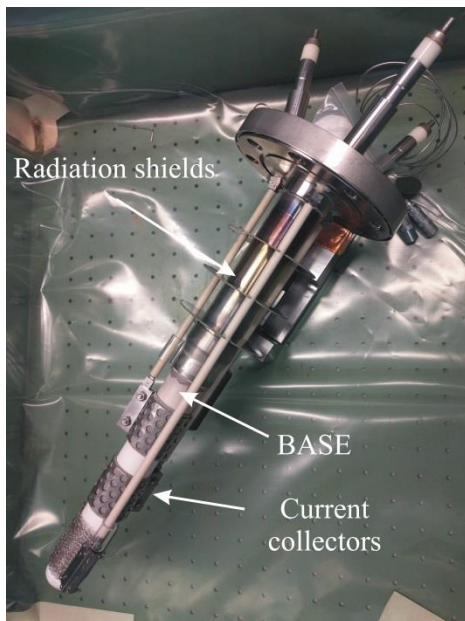
Figure 7. Central flange of the AMTEC test cell with the ceramic electrolyte as main component.

Electrically isolated feedthroughs are provided to lead the current in and out of the cell. Miniature feedthroughs have also been embedded for the thermocouples and heater at the upper flange. These were electrically isolated. Thermocouples were also placed at the condenser and were introduced through the outer cell containment. In the presented prototype BASE and condenser are located coaxially. To reduce radiation losses shielding sheets were placed in both sides of the cell and the inner wall of the condenser was polished.

During the assembly phase of the cell, special attention was paid to the development of a high-temperature ceramic to metal brazing and the coating of the BASE electrolyte. These two issues are presented in chapter 4. Also a thermal and stress evaluation of the assembly was performed using the ANSYS V14.5 software. The main goals were: i) the verification of the cell design for the AMTEC operating conditions and ii) identification of pressure and temperature limits of the structure. Results have been reported in [12] and show that no material failure should occur in the test cell, since all safety factors determined are sufficiently large above unity. The upper brazing between the niobium transition part and the metallic tube was determined to be the weakest component in the cell, due to the difference in the thermal expansion of the materials.

3.3. Data acquisition and control system

All the instrumentation of ATEFA is located in the test cell, sodium system and the immediately attached argon system. For a better evaluation of the temperature distribution in the cell, six different cross section planes were chosen to measure temperature difference in the radial direction, between anode and condenser. In the sodium system several thermocouples were placed to control the heat tracing system of the facility. Four absolute-pressure transmitters and a vacuum transmitter were located in the experimental facility in the argon system.

The cell and each of the tanks and were supplied with level sensors. The miniature level sensor developed for the cell was tested in the glovebox in hot sodium at 250 °C and showed a rapid reaction to sodium level changes and good wetting conditions even at moderate oxide layered free surface.. Moreover tests showed the validity of this sensor even with a moderate sodium oxide layer. Two scales were located below the sodium tanks to measure changes in the weight of the tanks, therefore the transport of sodium between tanks can be supervised. To measure the characteristic curve of the cell an electronic load is used, which adapts the electric circuit for different currents.

ATEFA is equipped with several heaters distributed all over the sodium system. The distribution was established depending on temperature range and also by design, which allows separable cell, valves and tanks. Different heating circuits regulate the power of the heaters in the system depending on the temperature regime and the heat capacity of each part. The total power needed for the heating system of the facility at steady state conditions is about 1.5 kW. The automatic control of the supplied heat power was done in the PC using a PID controller. For the monitoring of the data acquisition and control system a program was developed using LabView software and connected to the TwinCAT3 system Manager of the Beckhoff modules via Automation Device Specification (ADS) communication. In addition, the LabView software allows simulating the operational steps in ATEFA, which helped to optimize the control system.

Figure 8 shows the main states of the facility during operation and the respective transition processes. The facility starts at cold conditions T_{Na}<100 °C (first two states "system on/off") then it is cleaned from air and moisture and heated up to T_{Na} ~ 200 °C ("system clean"). The filling of the cell is first done at moderate temperatures T_{Na} ~ 200 °C ("cell full") and finally pressure and temperature are adjusted to the AMTEC conditions up to 800 - 1000 °C ("cell ready"). Finally the cell is operating after closing the electric circuit ("cell operating"). The draining of the facility is facilitated through pressurized argon and is supervised through temperature and pressure measurements in the facility. During maintenance and before filling up the cell/facility, the AMTEC test cell and sodium tanks can be physically disconnected from the facility for examination or refill after shutting down the system. Several subroutines have been programmed to be executed independently from the state or transition, for instance the constant automatic monitoring of temperature and pressure in the sodium system.

In case of a sodium leakage "emergency shutdown" will be initiated; automatically the complete heating system and the electric circuit of the cell will be switched off; and the outlet valves will start the floating process of the sodium containment with argon, so that any possible sodium fire can be extinguished. Simultaneously the facility will be depressurized.
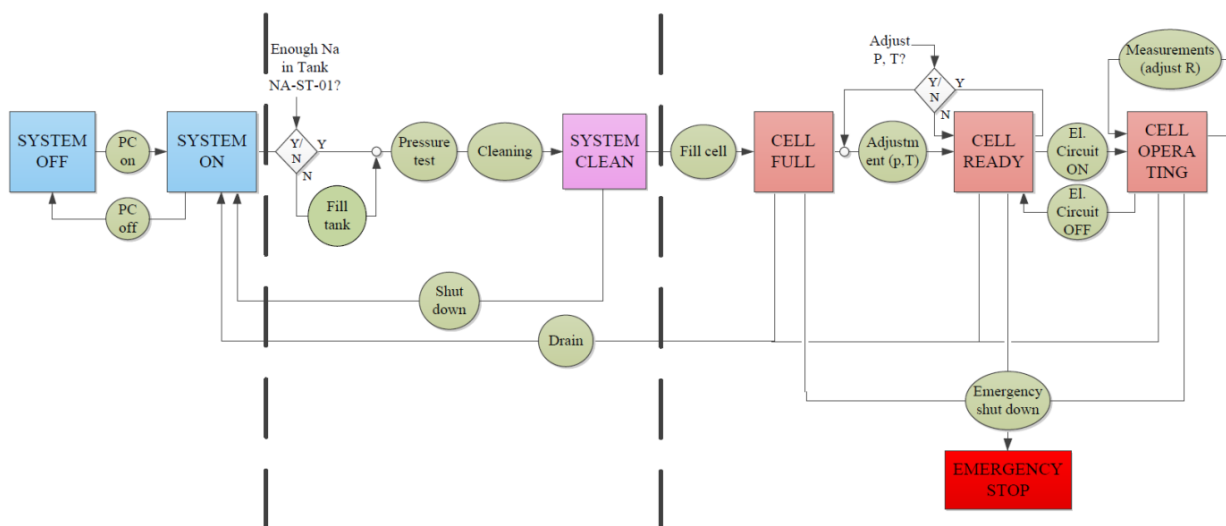
Figure 8. Process diagram of ATEFA. The boxes symbolize the stable states of the facility during operation and the green circles represent the transition processes between the states.

4. Key technology developments
The ceramic to metal joint and the magnetron sputtering of cathode layers on the BASE belong to the main key technology developments in this work.

4.1. Ceramic to metal joint

Active brazing is a one-step process where a specifically designed brazing filler metal is placed directly between two main materials and then heated in vacuum or in an inert atmosphere to avoid oxidation. The brazing filler material contains a reactive element to guarantee a good wetting by chemical reaction with the ceramic. Optimum brazing filler metals must have a low viscosity to ensure a good capillary action and provide a good distribution over the brazing area, a low surface tension to provide a good wetting of the joint surfaces, a reduced surface tension and a low volatilization of alloying elements of the brazing filler metals at brazing temperatures. Further, for a good quality of the brazing an adequate surface preparation; a proper joint design and clearance; and a proper brazing time and temperature are fundamental for a good quality braze.

TiCuNi brazing filler metal was tested by Williams et al. [5] and Knödler et al. [15]. In both cases the brazing was not recommended for high temperature (> 800 °C) AMTEC cells, due to the volatility and high solubility of Cu in Na. In the nineties at KIT (former Forschungszentrum Karlsruhe) Cu was substituted with Nb. Nb helped to reduce the thermal stresses due its thermal expansion coefficient similar to that of BASE. Among the joints tested in literature [5, 15] it was observed that Ti reacted strongly with the BASE. However the processes occurring in the brazing are still not completely understood; therefore further analysis and technology development is needed.

The brazing presented in this work has been developed at the Institute for Pulsed Power and Microwave Technology (IHM) [26]. It consists of a Ni-based brazing filler metal that includes a certain amount of Nb and Ti. The Nb particles act as filler particles in the wide gap and Ti particles were used as active material in the brazing for a good interaction with the ceramic. Tests revealed a strong influence of the gap size on strength and quality of the brazing. Optimization efforts were performed by decreasing significantly the tolerances of the ceramic. A helium leak tightness of 10^{-5} mbar l/s was achieved at the best ceramic-Nb brazing. Optimizations on the brazing are foreseen in ATEFA under AMTEC conditions, where the effects of the high temperature and the corrosion in sodium environment are considered.

4.2. Magnetron sputtering of cathode layers

The magnetron sputtered cathode layer on the BASE component is being developed at the Institute for Applied Materials – Applied Materials Physics (IAM-AWP). Titanium nitride and titanium carbide samples have been obtained using reactive d.c. magnetron sputtering [26]. A picture of a TiC coated BASE ceramic is presented in Figure 9.

Figure 9. BASE ceramic coated with TiC sputtered layer and connected to the niobium transition tube through a Ni-based braze filler material.
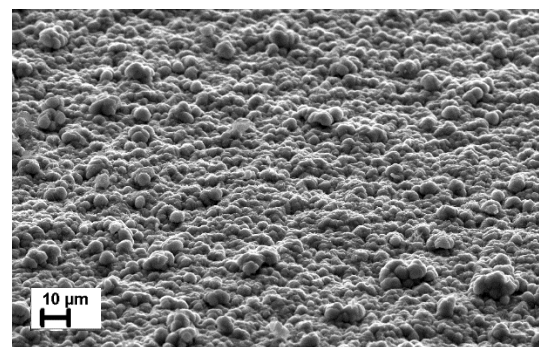
Figure 10. SEM top-view image of the TiC sputtering layer on BASE electrolyte.

Several of the magnetron sputtered electrode layers were analysed using the 4 point probe technique to measure the electrical sheet resistance of the electrode surface by using the correction factor described in [28]. A comparison of one of the TiN coated samples and two of the TiC coated samples developed in this work and the literature can be found in Table 3. As can be observed, results

obtained for the TiN coating show a developed sputtering layer with a significant low resistance. The sheet resistance of TiC layers could be reduced by a factor of 10 (TiC-2 compared to TiC-1) mainly by an increase of the layer thickness, which was one of the optimized parameters. The homogeneity of the layer thickness distribution seems to play an essential role considering the large surface roughness of the ceramic.

Despite the larger electrical resistivity of bulk TiC compared to the rest of the analysed materials, it shows very good results in thin sputtered layer configuration. A direct comparison of the sheet resistances between materials should be done taking into consideration the layer thickness and the porosity; unfortunately parameters like porosity are not easy to measure and are therefore rare to be found in the literature.

Some TiC coated BASE samples were analysed using the scanning electron microscope (SEM). Figure 10 shows exemplarily a top-view image of a coated electrode. Some parts of the TiC layer had been detached after several hours/days, therefore the microscopic structure was not perfectly homogeneous. Possible causes of the moderate adhesion may lie on: i) the surface quality of the BASE, ii) pretreatment before the coating (cleaning, brazing, etc.) and/or iii) coating process. The high chemical reactivity of BASE to absorb for instance moisture makes the handling process difficult. Further optimization and analysis is therefore needed.

Table 3. Comparison of measured sheet resistance of AMTEC electrodes for different materials.

Sputter-Layer	ρ_{bulk} (20 °C) [10^{-8} Ωm]	ρ_{sheet} [$\Omega/\square$]	t_e [µm]	Ref.
Mo	5.5	11…16	-	16
WPt	W 5.5 Pt 10.3	18.8…98.1	0.7…1	22
WRh	W 5.5 Rh ~5	40.9…92.1	0.7…1	22
NbN	Nb 15	20…100	2…3	29
TiN-1 TiN-2	20	13.8…19.1 17.7…4.1	1.1…1.3 0.9…2.0	30
TiN TiC-1 TiC-2	20 60	0.18…0.70 132…351 21…24	- TiC-1 < TiC-2 TiC-2 ≤ 5	This work

5. Conclusions

The aim of the present work was to present the layout and engineering solutions, the construction of ATEFA and the AMTEC test cell using new technologies available in KIT. The research was focused on AMTEC systems intended to be applied in concentrating solar power plants. The main components of the cell have been addressed and analysed: BASE, electrodes, current collectors and working fluid. In addition technology developments achieved in the field of ceramic-to-metal brazing and electrode coating of BASE ceramics were addressed, including the analysis of the electrode samples.

Acknowledgments

References

[1]   Hering W, Stieglitz R and Wetzel T 2012 *EPJ Web of Conf.* 33:03003.1–7
[2]   Hering W, Diez de los Rios Ramos N, Onea A and Stieglitz R 2016 *Proc.10th PAMIR Int. Conf. (Cagliari)*
[3]   Onea A, Hering W, Reiser J, Weisenburger A, Diez de los Rios Ramos N, Lux M, Ziegler R, Baumgärtner S and Stieglitz R 2017 *IOP Conf. Ser.: Mater. Sci. Eng.*
[4]   Heinzel V, Huber F, Peppler W and Will H 1991 *J. Mat. Science For.* **76** 261–4
[5]   Williams R M, Ryan M A, Jeffries-Nakamura B, Underwood M L, O'Connor D and Kikkert S 1991 *Proc. 8th Symp. on Space Nuclear Power Systems* 464–71
[6]   Heinzel V, Huber F, Peppler W and H. Will 1991 *J. Key Eng. Mater.* **59–60** 381–394
[7]   Lodhi M A K, Vijayaraghavan P and Daloglu A 2001 *J. Power Sources* **96** 343–51
[8]   Hunt T K and Rasmussen J R 2006 *AIP Conf. Proc.* **813** 567–72
[9]   Hunt T K 1986 *Proc. Worksh. on Solar Appl.of En. Conv. Tech.* 65-77.
[10]   Williams R M, Loveland M E, Jeffries-Nakamura B, Underwood M L, Bankston C P, Leduc H and Kummer J T 1990 *J. Electr. Soc.* **137** 1709-15
[11]   Koganei K, Oyama T, Inada M, Enomoto N and Hayshi K 2014 *Solid State Ionics* **267** 22–6
[12]   Onea A, Diez de los Rios Ramos N, Hering W, Palacios J L and Stieglitz R 2015 *Magnetohydrodynamics* **51** 249–61
[13]   Kato A, Nakata H and Tsuchida K 1993 *Proc. 28th IECEC* **1** 1.819–22
[14]   Knödler R, Reiss K and Westhoven B 1992 *J. Mat. Science Lett.* **11** 343–5
[15]   Knödler R, Bossmann H P, Kranzmann A and Harbach F 1992 *J. Electr. Soc.* **139** 3029–34
[16]   Underwood M L, Williams R M, Jeffries-Nakamura B, Bankston C P and Cole T 1988 *Proc. 23rd IECEC* **1** 227–33
[17]   Hunt T 1990 *Proc. 25th IECEC* 420–5
[18]   Fang Q and Knödler R 1992 *J. Mat. Sci.* **27** 6725–9
[19]   Fletcher R W and Schwank 2003 J W *AIP Conf. Proc.* **654:1** 722–9
[20]   Wheeler B L, Williams R M, Jeffries-Nakamura B, Lamb J L, Loveland M E, Bankston C P, and Cole T 1988 *J. App. Electrochemistry* **18** 410–6
[21]   Ryan M A, Jeffries-Nakamura B, Williams R M, Underwood M L, O'Connor D and Kikkert S 1991 *Proc. 26th IECEC* **5** 463–8
[22]   Williams R M , Jeffries-Nakamura B, Underwood M L, Wheeler B L, Loveland M E, Kikkert S J, Lamb J L, Cole T, Kummer J T and Bankston C P 1989 *J. Electr. Soc.* **136** 893–4
[23]   Tsuchida K, Nagata T, Nakata H and Kato A 1998 *J. Mat. Sci.* **33** 755–62
[24]   Virkar A V, Jue J F and Fung K Z 2000 *Alkali-metal-ß- and ß''-alumina and gallate polycrystalline ceramics and fabrication by a vapor phase method* Patent (United States) 6,117,807
[25]   Diez de los Rios Ramos N, Onea A, Scherrer S, Weisenburger A and Hering W 2015 *Proc. 5th Int. Youth Conf. Energy (Pisa)*
[26]   Diez de los Rios Ramos N, Weisenburger A, Onea A, Hering W, Stüber M, Ulrich S and Stieglitz R 2016 *Proc. 10th PAMIR Int. Conf. (Cagliari)*
[27]   Onea A, Hering W, Lux M and Stieglitz R 2017 *Int. J. Heat Mass Transfer* **113** 984
[28]   Smits F M 1958 *Bell System Tech. J.* **37:3** 711–8
[29]   Kato A, Tsuchida K, Hashimoto T, Nakata H and Nagata T 1992 *Proc. 27th IECEC* **3** 3.1–6
[30]   Asakami O, Tsuchida K and Kato A. 1990 *J. Mat. Sci. Lett.* **9** 892–4